Modeling the Effects of Mutations on the Free Energy of the First Electron Transfer from Q_A^- to Q_B in Photosynthetic Reaction Centers†

E. Alexov,‡ J. Miksovska,§ L.Baciou,§ M. Schiffer,|| D. K. Hanson,|| P. Sebban,§ and M. R. Gunner*,‡

Department of Physics, City College of New York, 138 Street & Convent Avenue, New York, New York 10031, Centre de Genetique Moleculaire, Bat. 24, CNRS, 91198 Gif/Yvette, France, and Biosciences Division, Argonne National Laboratory, 9700 South Cass Avenue, Illinois 60439

Received December 23, 1999; Revised Manuscript Received February 14, 2000

ABSTRACT: Numerical calculations of the free energy of the first electron transfer in genetically modified reaction centers from *Rhodobacter* (*Rb.*) *sphaeroides* and *Rb. capsulatus* were carried out from pH 5 to 11. The multiconformation continuum electrostatics (MCCE) method allows side chain, ligand, and water reorientation to be embedded in the calculations of the Boltzmann distribution of cofactor and amino acid ionization states. The mutation sites whose effects have been modeled are L212 and L213 (the L polypeptide) and two in the M polypeptide, M43(44) and M231(233) in *Rb. capsulatus* (*Rb. sphaeroides*). The results of the calculations were compared to the experimental data, and very good agreement was found especially at neutral pH. Each mutation removes or introduces ionizable residues, but the protein maintains a net charge close to that in native RCs through ionization changes in nearby residues. This reduces the effect of mutation and makes the changes in state free energy smaller than would be found in a rigid protein. The state energy of $Q_A^-Q_B$ and $Q_AQ_B^-$ states have contributions from interactions among the residues as well as with the quinone which is ionized. For example, removing L213Asp, located in the Q_B pocket, predominantly changes the free energy of the $Q_A^-Q_B$ state, where the Asp is ionized in native RCs rather than the $Q_AQ_B^-$ state, where it is neutral. Side chain, hydroxyl, and water rearrangements due to each of the mutations have also been calculated showing water occupancy changes during the Q_A^- to Q_B electron transfer.

In photosynthetic bacteria, the conversion of light into chemical free energy takes place in the reaction center protein (RCs).[1] The energy of an absorbed photon initiates a transmembrane charge separation reaction. The initial excitation of the primary electron donor, a dimer of bacteriochlorophylls (P), situated near the periplasmic side of the protein results, within 200 ps, in the reduction of the primary quinone electron acceptor, Q_A, situated on the cytoplasmic side of the protein. Q_A then reduces the secondary quinone, Q_B in <100 μs (*1*−*3*). In isolated RCs, neither Q_A^- nor Q_B^- is protonated (*4*). However, semiquinone formation causes substoichiometric proton uptake by ionizable residues which change their ionization states in response to the negative charge on Q_A and/or Q_B (*5*, *6*). Q_A acts as a one electron carrier, while Q_B functions as a two electron gate (*7*). The transfer of two successive electrons to Q_B 15 Å, from the protein surface, is coupled to its double protonation with the uptake of two protons from the cytoplasm via the protein matrix. The dihydroquinone, Q_BH_2, is then released from the RCs and replaced by an oxidized ubiquinone from the membrane. In *Rhodobacter* (*Rb.) sphaeroides* and *Rb. capsulatus* RCs, Q_A and Q_B are both ubiquinone-10. Thus, their different functional behaviors must arise from their different protein environments (*8*). For example, Q_B is more closely surrounded by ionizable residues than is Q_A (*9*−*11*).

High-resolution three-dimensional structures are available for RCs from *Rb. sphaeroides* (2.2 Å resolution) (*9*, *12*) and *Rps. viridis* (2.3 Å resolution) (*11*, *13*). The protein possesses at least three polypeptides, L, M, and H, with molecular masses between 30 and 35 kDa. The L and M subunits carry all pigments and cofactors involved in the primary charge separation process. Q_A is associated with the M and Q_B with the L subunits. There is a high degree of sequence homology between the proteins from these different organisms. *Rb. sphaeroides* RCs have 72% identity with those of *Rb. capsulatus* and 49% sequence identity with those of *Rps. viridis* (*14*). The major structural features are conserved between the RCs of *Rb. sphaeroides* and *Rps. viridis* (*15*). It is likely that the *Rb. capsulatus* structure is more similar to the protein from *Rb. sphaeroides* with which it shares much higher sequence identity (*16*). The functional behavior of the RCs from both species is found to be very similar (see reviews in refs *17*−*21*).

† We are grateful for the financial support of HFSO Grant RG-329/95, NSF MCB 9629047 and NATO Grant (LST.CLG 975754). D.K.H. and M.S. are supported by the U.S. Department of Energy, Office of Biological and Environmental Research, under Contract W-31-109-ENG-38.

* To whom correspondence should be addressed. Phone: (212) 650-5567. Fax: (212) 650-6940. E-mail: gunner@sci.ccny.cuny.edu.

‡ City College of New York.

§ Centre de Genetique Moleculaire.

|| Argonne National Laboratory.

[1] Abbreviations: P, bacteriochlorophyll dimer; H_L, bacteriopheophytin near Q_A in the active L branch of the protein; UQ, Ubiquinone-10; RC, reaction center; Q_A and Q_B, primary and secondary electron acceptor quinones. Residue numbering: *Rb. capsulatus* (*Rb. sphaeroides* if different); WT, wild type RC.

10.1021/bi9929498 CCC: $19.00
Published on Web 00/00/0000 PAGE EST: 12.5

Numerical calculations based on the three-dimensional structure of wild-type RCs have been used to explore the relative importance of individual residues in modulating the free energy of the first electron transfer from Q_A^- to Q_B ($-\Delta G_{AB}$) and in defining the pathways for proton uptake and delivery (*22*−*27*). Computational analysis of mutant proteins adds to the picture of how RCs work providing an atomic level explanation for the measured results. For example, removing an important residue within a cluster of strongly interacting groups may have little effect on the measured reaction, because other residues can compensate for its absence. In addition, spectroscopic data alone cannot determine if a mutation that changes the reaction driving force modifies the reactant or the product states or both. Appropriate calculations can distinguish between these alternatives and can more accurately highlight the role of the individual residues. Both the static influence of the protein in tuning the electrostatic environment of the quinones and the ionizable residues as well as the role of protein reorganization following the formation of each new redox state can be considered (*25*).

Simultaneous calculation of both ionization and conformation states has been attempted by a number of methods (*22*) and reviews (*66*−*68*). The earliest methods averaged interactions between different possible side chain atomic positions (*69*) and then used the obtained ionization states in standard molecular dynamics calculations (*28*), or they averaged the ionization states calculated for different structures (*70*, *71*). New methods combine conformation changes and calculations of ionizable states (*25*, *30*, *72*). Recently, an iterative mobile cluster approach was used to calculate multiple-site ligand binding to flexible macromolecules (*29*). The multiconformation continuum electrostatics (MCCE) procedure allows multiple positions of hydroxyl and water protons, alternative side-chain rotamers, water positions, and ligand positions in the calculation of the pH dependence of the ionization equilibria of titratable groups (*25*, *30*).

The recent analysis of WT *Rb. sphaeroides* with the MCCE method has provided a good match with experimental data for the $-\Delta G_{AB}$ and protein uptake on the formation of Q_A^- or of Q_B^-. The MCCE method combines calculation of the ionization states and conformation changes of the protein as a function of the cofactor ionization state and pH (*25*, *30*). Side chains, cofactors, and buried water molecules have preassigned alternate positions and charges. Each of these choices for a given residue charge and position is called a conformer. Acidic and basic residues have ionized and neutral conformers. Neutral acids, hydroxyl residues, and waters have conformers with different proton positions. Buried waters can have their oxygens in alternate positions within a binding site. Each microstate of the protein has one conformer for each residue, cofactor, and water. Monte Carlo sampling calculates the probability of realizing each of the initially suggested conformers in a Boltzmann distribution of microstates. The strength of the MCCE method is that atomic positions and ionization states are allowed to come to equilibrium in a single, self-consistent calculation. Previous work showed that for many residues several atomic positions are significantly occupied in the Boltzmann distribution of RC microstates (*25*). A cluster of strongly interacting residues (L210Asp, L212Glu, L213Asp, and SerL223) was found to play an important role in the electron transfer from Q_A^- to Q_B.

The functional properties of RCs with mutations at the site of either of two acidic residues, L213Asp and L212Glu, have been extensively investigated in *Rb. capsulatus* (*31*) and *Rb. sphaeroides* (*32*, *33*) RCs. Similar results are found in both species. In *Rb. sphaeroides*, L213Asp (situated 5 Å from Q_B) was shown to be of crucial importance for the delivery of the first proton to Q_B (*34*, *35*). Its removal changes the free-energy gap between $Q_A^-Q_B$ and $Q_AQ_B^-$ states stabilizing the product ($\Delta G_{AB} = -110$ meV), by about 50 meV from that found in WT RCs ($\Delta G_{AB} = -60$ meV) (*34*, *35*). The removal of L213Asp also changes the pH dependence of the free energy. In native RCs the reaction is pH independent (pH 6−8) and became less favorable at higher pH and more favorable at low pH, while in RCs lacking L213Asp, the free energy is practically pH independent until high pHs. Theoretical calculations have found that L213Asp is ionized at physiological pH in the ground and $Q_A^-Q_B$ states and is protonated in the $Q_AQ_B^-$ state (*23*, *25*, *26*).

L212Glu, situated 6 Å from Q_B, is involved in the transfer of the second proton to the doubly reduced quinone (*33*, *36*−*38*). In contrast to the L213Asp → Asn mutation, changing L212Glu to the neutral Gln has little effect on the free-energy gap for the Q_A^- to Q_B electron-transfer reaction. In addition, at neutral pH, the amplitude of the proton uptake on Q_B reduction in the L212Glu → Gln mutant was found to be the same as in the WT RCs. These results led to the suggestion that L212Glu is protonated at neutral pH in isolated RCs (*37*, *38*). Such a high pK_a for L212Glu is reasonable if the nearby L213Asp is ionized (*37*). Previous MCCE calculations found that L212Glu is protonated in the ground state. However, data from FTIR suggest that L212Glu is partially ionized in the ground state (*39*). Experimental data obtained in different *Rb. Sphaeroides* mutants lacking L212Glu have shown that the proton uptake on Q_A reduction is sensitive to mutations at L212 (*40*, *41*). Thus, the role of L212Glu seen in FTIR experiments (*39*, *42*, *43*) and in current MCCE calculations is the most significant disagreement between calculations and experiment. This discrepancy can be caused by protein rearrangement that is not included in the model.

Replacing L212Glu or L213Asp with other residues yields photosynthetically incompetent strains (*21*). Some photocompetent phenotypic revertants derived from strains lacking L213Asp and L212Glu carry compensating mutations that are situated 10−15 Å away from Q_B (*44*). Second-site mutations of *Rb. capsulatus* RCs lacking L212Glu and/or L213Asp which are considered in this paper are M43(44)Asn → Asp and M231(233)Arg → Leu (*31*, *45*) [Residue numbering: *Rb. capsulatus* (*Rb. sphaeroides* if different)]. Each compensatory mutation substitutes a residue that reduces the charge change introduced on removing the two acidic residues. This result highlights the importance of electrostatic interactions in the Q_B site of RCs (*31*, *46*). The mutated strains which are considered here are (i) single mutants L212EQ (L212Glu → Gln), L212EA (L212Glu → Ala), M43(44)ND [M43(44)Asn → Asp], and M231(233)RL [M231(233)Arg → Leu]; (ii) double mutant L212EA−L213EA ("AA"); (iii) and phenotypic revertants carrying second-site suppressor mutations AA + M43(44)ND and AA + M231(233)RL. To interpret further the results of modeling the AA double mutant, calculations were also carried out

for single mutant L213DA (L213Asp → Ala); this mutant has not yet been constructed. Results can be compared with the L213Asp → Asn mutant (*34*, *35*). The numerical analysis focuses on transfer of the first electron from Q_A^- to Q_B. The calculations use coordinates of RC from *Rb. sphaeroides* as no structure is available for the *Rb. capsulatus* RC.

METHODS

MCCE Method. The MCCE procedure requires three main steps: (1) generating a coordinate file containing alternative ionization and positional conformers; (2) calculating self- and pairwise electrostatic and nonelectrostatic energies for each conformer; (3) calculating the equilibrium population of all conformers and the free energy of the protein in different redox states. The method has been described in detail for calculations of the free energy of the electron transfer from Q_A^- to Q_B from pH 5 to 11 in WT *Rb. sphaeroides* RCs (*25*).

(1) Generation of the Coordinate File. The MCCE method requires a single composite protein data file with all conformers present. The coordinate file was build up as described in ref *25*. This provides 1726 conformers for generating different ionization states and atomic positions. Although extra side chains were taken from available alternative crystal structures, the method is not restricted to this technique. A more recent implementation of the MCCE method (Alexov, E., Karpman, D., and Gunner, M. R., in preparation) generates side-chain rotamers automatically providing library rotamers for residues (*47*−*49*). Additionally, more detailed charge set distribution can be used for cofactors (*27*). These were not added here. Rather, the same structure used in ref *25* was retained to allow direct comparison with previous studies of WT RCs.

Mutations were introduced in the structure by generating additional side chains at the appropriate positions on the WT backbone. Coordinates of the mutated amino acids were built using the Turbo-Frodo program (*47*). Thus, in addition to the L212Glu side-chain coordinates, the generated file contains additional atom coordinates for L212Gln and L212Ala. One extra conformer at position L213 for the L213A mutant was introduced. At position M43(44)Asn, two extra conformers for ionized and neutral Asp were added. Finally in addition to the conformer of the native M231-(233)Arg, one extra conformer accounts for the side chain of Leu. This brings the total number of conformers to 1732. Calculations on a given mutant protein only use the appropriate conformers of each residue.

(2) Calculation of Conformer Self- and Pairwise Energies. The energy of each microstate is made up of self-and pairwise electrostatic and nonelectrostatics energies for all conformers contained in the microstate (*25*, *30*). These values are calculated prior to Monte Carlo sampling.

Electrostatic energies are calculated with the program DelPhi (*50*, *51*) using the finite-difference technique to solve the Poisson−Boltzmann equation. Parse charges and atomic radii (*52*) are used and cofactor charges were taken from ref *53*. The iron atom has a charge of +2. The histidine ligands are considered to have the charge distribution of neutral histidine. The charges on the quinones are taken from ref *24*. The dielectric constant values of 4 and 80, respectively, are used for the protein and the bulk water. The salt concentration is zero. One DelPhi run provides three energy terms for each conformer (i): (1) the loss of reaction field (desolvation) energy $\Delta G_{\mathrm{rxn},i}$ for each conformer in its position in the protein; (2) the polar interaction energy $\Delta G_{\mathrm{pol},i}$, which is the sum of all pairwise electrostatic energies between the side chain of the ith conformer and the backbone and the side chains with no conformational degrees of freedom; (3) the pairwise interactions between i and other conformers (j) in the protein $\Delta G_{\mathrm{el}}^{ij}$. $\Delta G_{\mathrm{rxn},i}$, and $\Delta G_{\mathrm{pol},i}$ are collected into two vectors of length M, where M is the number of conformers. $\Delta G_{\mathrm{el}}^{ij}$ is collected into a $M \times M$ matrix.

Nonelectrostatic Lennard-Jones and torsion energies for each conformer were calculated as described previously using the same parameters (*25*). For the ith conformer $\Delta G_{\mathrm{nonel},i}$ includes the torsion energy and Lennard-Jones interactions with parts of the protein without conformational degrees of freedom. The pairwise Lennard-Jones energies of interaction between conformer i and j result in a $M \times M$ matrix ($\Delta G_{\mathrm{nonel}}^{ij}$).

The energy of a given microstate is the sum of electrostatic and nonelectrostatic energies for the conformers included in the microstate n:

$$\Delta G^n = \sum_{i=1}^{M} \delta_n(i)\{\gamma(i)[2.3k_BT(\mathrm{pH} - \mathrm{pK}_{\mathrm{sol},i})] + [\Delta G_{\mathrm{rxn},i} + \Delta G_{\mathrm{pol},i} + \Delta \mathrm{G}_{\mathrm{none},i}]\} + \sum_{i=1}^{M} \delta_n(i) \sum_{i=1}^{M} \delta_n(j)[\Delta G_{\mathrm{el}}^{ij} + \Delta G_{\mathrm{nonel}}^{ij}] \quad (1)$$

where k_BT is 0.59 kcal/mol (25.8 meV), M is the number of conformers, $\delta_n(i)$ is 1 for conformers that are present in the microstate n and 0 for all others. $\gamma(i)$ is 1 for bases, −1 for acids, and 0 for polar groups and waters. $pK_{\mathrm{sol},i}$ is the pK_a of the ith group in solution. The free energy of transferring the water into the protein was taken as 5.3 kcal/mol, which corresponds to the 1.5 mM solubility of water in cyclohexane plus the cost of opening a cavity in the protein (0.7 kcal/mol) (*54*).

(3) Monte Carlo Calculations. The number of microstates is $\prod_{i=1}^{N} L_i$, where N is the sites with conformational flexibility (528) and L_i the number of conformers per site i (ranging from 2 to a maximum of 20 for some waters). It is clearly impossible to obtain the desired thermodynamic parameters by a statistical mechanical analysis that would require enumerating all microstates. Rather 40 million steps of Monte Carlo sampling were carried out to determine the Boltzmann distribution of conformers for each mutant, in each RC redox state, at each pH.

The simulation of each redox state for each mutant is achieved by restricting particular conformers in a given Monte Carlo calculation. Thus, all conformations are included in the energy vectors and matrixes described above. However, an individual conformer for a particular residue or cofactor can be required or disallowed in a given simulation. In the ground state of a WT protein, no microstates with Q_A, Q_B, or P having charge are allowed. In addition, all alternate residue type conformers that are included for the analysis of the mutants are disallowed. All other conformers can then be formed into possible microstates.

The $Q_A^-Q_B/Q_AQ_B^-$ equilibrium constant was obtained from calculations where all microstates have either Q_A^- or Q_B^- but never both. In the calculations, P was constrained to be P^+ as it is in measurements of the equilibrium constant by the charge recombination technique (*55*). The pH of the calculations was varied by changing its value in eq 1. No explicit restriction on allowed conformers was made as the pH changes. Calculations were also performed at pH 7 with the protein in the following redox states: the ground state: all cofactors neutral; $P^0Q_A^-Q_B$, Q_A is negatively charged; $P^+Q_A^-Q_B$, P has a positive charge and Q_A a negative charge; $P^0Q_AQ_B^-$, Q_B is negative; and P^+ $Q_AQ_B^-$, P has a positive and Q_B a negative charge. Calculations for each mutant protein restricted the conformers included in the sampled microstates. For example, where L212Glu is changed to Gln, neutral or ionized conformers of Glu are forbidden while a conformer of Gln at L212 must be occupied. Monte Carlo sampling thus allows all other side-chain position and ionization conformers to come to equilibrium in each mutant, in each redox state, at each pH.

(4) Calculation of the Free Energy ($-\Delta G_{AB}$) of the Electron Transfer from Q_A^- to Q_B. The free energy of the electron transfer from Q_A^- to Q_B was calculated from the equilibrium constant (K_{eq}), which is given by the ratio of occupancies of the Q_B^- (ρ_B) and the Q_A^- (ρ_A) states in a Monte Carlo run where one quinone but not both is reduced in each microstate. The distribution of reduced quinone is therefore dependent on the relative energy of the entire ensemble of microstates that contain the electron on a particular quinone. Thus

$$\Delta G_{AB}^{calc} = -k_B T \ln K_{eq} = -k_B T \ln \frac{\rho_B}{\rho_A} \qquad (2)$$

Three Monte Carlo runs were carried out at each pH for each mutant. The results were averaged and standard deviations calculated to provide the error bars for values of $-\Delta G_{AB}$. The errors come from the uncertainty of the Monte Carlo method especially in large systems with rough energy landscapes as in the system considered here.

The $\Delta\Delta G_{AB}$ difference between WT and particular mutant is given by

$$\Delta\Delta G_{AB} = \Delta G_{AB}^{WT} - \Delta G_{AB}^{mutant} \qquad (3)$$

(5) Determining $-\Delta G_{AB}^{exp}$. All procedures concerning the construction of the *Rb. capsulatus* mutants, isolation, and genotypic characterization of the phenotypic revertant strains, and purification of the reaction centers have previously been described (*38*, *44*, *56*).

The $-\Delta G_{AB}^{exp}$ values were deduced from the measurements (at 865 nm) of the P^+ Q_A^- (k_{AP}) and P^+ Q_B^- (k_{BP}) charge recombination rates as given by (*57*, *58*)

$$-\Delta G_{AB}^{exp} = -kT \ln(k_{AP}/k_{BP} - 1) \qquad (5)$$

In RCs where k_{BP} is small, charge recombination from P^+ $Q_AQ_B^-$ to the ground state may occur by direct electron transfer from Q_B^- to P^+, rather than through the P^+ Q_A^- state (*59*). The calculated $-\Delta G_{AB}^{exp}$ value may be underestimated in these cases. However, as will be seen, comparison of experimental and calculated values of $-\Delta G_{AB}$ for the whole set of modified RCs is consistent with a negligible deviation from formula 5 for any mutant.

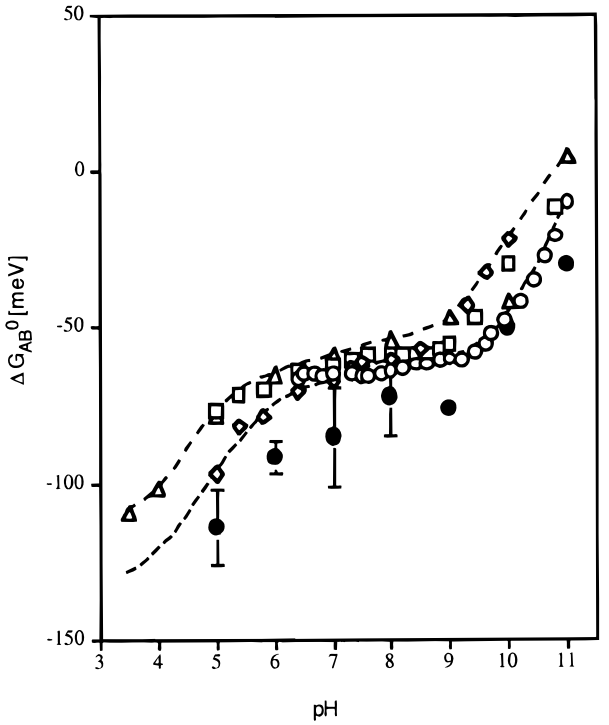

FIGURE 1: pH titration of the free energy of the first electron transfer from Q_A^- to Q_B. Experimental data are taken from refs *5* (□), *55* (○), and *65* (◇) in *Rb. sphaeroides* and ref *56* (△) *Rb. capsulatus*. The broken lines represent the envelope of the experimental data. The calculated curve for $-\Delta G_{AB}$ for the WT RCs (●) (*25*).

RESULTS

Previous MCCE calculations have explored how the protein structure in WT *Rb. sphaeroides* RCs controls the free energy of the first electron transfer from Q_A^- to Q_B ($-\Delta G_{AB}$) as a function of pH (*25*). The comparison between the calculated $-\Delta G_{AB}$ and the range of the experimental curves measured in *Rb. sphaeroides* and *Rb. capsulatus* RCs is displayed in Figure 1. It can be seen that in native RCs the $-\Delta G_{AB}$ is approximately 60 meV at physiological pH, and it is practically pH independent in the pH range 5−8. This is consistent with the proton uptake on the first electron transfer from Q_A^- to Q_B being close to zero. Major ionization changes on electron transfer were found to be associated with L213Asp and L210Asp. L213Asp is fully ionized in the Q_A^- and fully protonated in the $Q_AQ_B^-$ states. The proton is taken from L210Asp, which is mostly protonated in the Q_A^- and fully ionized in the $Q_AQ_B^-$ states. Thus, the proton rearrangement occurs inside the protein, without requiring proton uptake from solution.

The results presented here discuss the calculations of the $-\Delta G_{AB}$ in several mutated RCs, comparing calculated and experimental values. This comparison of the pH dependence of $-\Delta G_{AB}$ will be divided into three pH regions: (1) 3.5−6 (low), (2) 6−8 (physiological, intermediate), and (3) 8−11 (high). All structures of RCs have been determined in crystals obtained at neutral pH (usually 6−7). Therefore, the most reliable calculations can be expected in this pH range. Nevertheless, the calculations have been carried out over the wide pH range to try to account for all the available

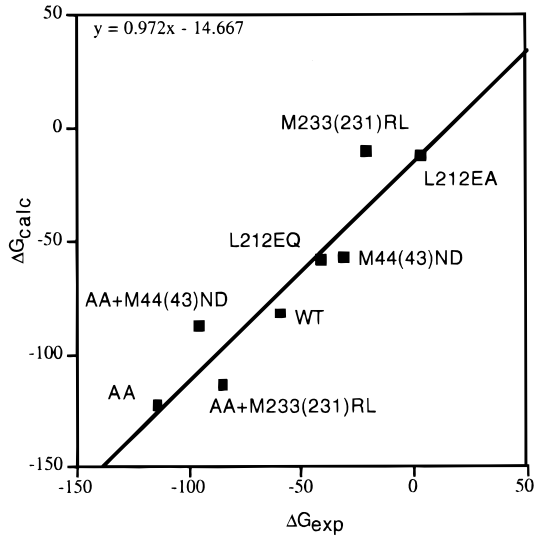

FIGURE 2: Calculated versus experimental $-\Delta G_{AB}$ for WT and mutant RCs. Residues are labeled by *Rb. capsulatus* sequence numbers, where different *Rb. sphaeroides* numbers are in parentheses.

experimental data. This tests if the residue side chain, cofactor, water, and hydroxyl flexibility in these MCCE calculations can account for the modifications of the protein structure at low and high pHs (see ref *25* for a more complete description of the errors in analysis at the extremes of pH).

The results of the calculations of the $-\Delta G_{AB}$ at pH 7 are plotted against the experimental data in Figure 2. It can be seen that the best fit is a line with slope almost 1 and with constant shift of about 15 meV. Three mutant substitutions make the first electron transfer more favorable, while four mutant substitutions destabilize the reaction. Although all mutations introduce or remove a potentially charged group, the $-\Delta G_{AB}$ changes by only about $\pm$60 meV compared to the native RC. As will be seen, the effects of the mutations are reduced by the protein rearrangements.

L212Glu → Gln Mutant. Previous experimental measurements achieved with the L212Glu → Gln mutant showed that $-\Delta G_{AB}$ is only slightly changed ($\sim$20 meV at pH 7) compared to native RCs in the low and intermediate pH ranges (*38*). As displayed in Figure 3a and Table 1, in this pH region, there is a good agreement between the calculated and the experimental $-\Delta G_{AB}$ values. Similar $-\Delta G_{AB}$ values were measured in *Rb. sphaeroides* L212Glu → Gln mutants (*33*, *37*). However, above pH 9 in the mutant, the experimental $-\Delta G_{AB}$ remains pH independent while in the calculations the mutant behaves like WT RCs. The experimental observation that $-\Delta G_{AB}$ for the WT and L212Glu → Gln RCs differ only slightly at pH 7 led to the suggestion that L212Glu is protonated at this pH in the ground, $Q_A^- Q_B$ and $Q_A Q_B^-$ states (*37*). This is consistent with the previous MCCE calculations of WT RCs (*25*). The small difference in the $-\Delta G_{AB}$ values in the mutant results from replacing the uncharged protonated Glu^0 by Gln. Detailed analysis of the protein ionization and conformation distribution in the mutant and WT RCs suggest there are almost identical pairwise interaction energies of the dipoles of Gln and Glu^0 with Q_A^- and Q_B^-, as well as with the surrounding residues. Indeed no group is calculated to change its distribution of positions or charge by more than 10% when Gln is substituted for Glu in the ground state at pH 7 (Table 1). Conformation and ionization changes in the first electron transfer from Q_A^- to Q_B are also the same as those in WT RCs (Table 2).

The calculated pH dependence of $-\Delta G_{AB}$ in the mutant and the WT is the same, because in the WT RCs, L212Glu remains neutral above pH 11. It may be that partial ionization of L212Glu in WT RCs at a pH above 9.5, missed in the calculations, accounts for the experimentally observed difference at high pH between the WT and the L212Glu → Gln mutant. Although as will be seen the calculations for several other mutants also show more pH dependence at high pH then is experimentally seen.

L212Glu → Ala Mutant. In the L212Ala mutant, the experimental $-\Delta G_{AB}$ (Figure 3a) at neutral pH is $\sim$60 meV less favorable than in WT RCs (*56*). In the L212Ala mutant, the experimental and calculated $-\Delta G_{AB}$ values are in good agreement in the low and medium pH ranges (Figure 3b, Table 1). At high pH, however, the calculations show somewhat more pH dependence than is measured.

Ala or Gln at position L212 produces different effects on $-\Delta G_{AB}$. Experimentally, the Ala mutant decreases $-\Delta G_{AB}$ by about 45 meV more than Gln. The electrostatic interactions of L212 Glu^0 or L212Gln with nearby residues were obtained from the input files for the calculation of microstate energies in the Monte Carlo sampling. These interactions will be absent in the L212Glu → Ala mutant. The pairwise interactions between L212Glu^0 or L212Gln and Q_A^-, Q_B^-, and the nearby residues L213Asp, L210Asp, and H173Glu contribute only $\sim$11 meV to $-\Delta G_{AB}$. Therefore, much of the difference between $-\Delta G_{AB}$ in the L212Glu → Ala and L212Glu → Gln mutants cannot be assigned to a significant change in a few local interactions. Rather it appears to be due to small contributions dispersed over many residues. No difference in conformer occupancy of WT RCs and the mutant was found at ground state and physiological pHs (Table 1).

Although the substitution of the dipole of Glu^0 by Ala destabilizes the $Q_A^- Q_B$ state relative to the $Q_A Q_B^-$ state, no changes of more than 10% are calculated in conformer occupancies between ground and the $Q_A^- Q_B$ states (Table 2). The ionization and conformation changes in the first electron transfer from Q_A^- to Q_B were the same as in WT RCs (Table 2).

L213Asp → Ala Mutant. The L213Asp → Ala single mutant has not been constructed, therefore no experimental data are available, but the results can be compared qualitatively to the L213Asp → Asn mutant (*34*, *35*), where the reaction is found to be $-$80 meV more favorable than in the WT RCs (*60*). However, the theoretical calculations were carried out with Ala here for comparison with the "AA" double mutant (L212Ala + L213Ala) discussed below (Figure 3c). At pH 7, in the L213Asp → Ala RCs, the calculated $-\Delta G_{AB}$ is $\sim$25 meV smaller than that calculated for WT RCs (Table 1,) and it is pH independent below pH 9. Above pH 9, $-\Delta G_{AB}$ decreases.

Two major differences in ionization states were found comparing WT and the mutant RCs in the ground state at physiological pHs (Table 1). L213Asp, which is fully ionized in the WT RCs, is removed in the mutant. Its negative charge is then transferred to L210Asp (75%) and to L212Glu (15%), which are 25% ionized (L210Asp) and fully (L212Glu) neutral in WT RCs. Thus, in the mutant, L210Asp is fully

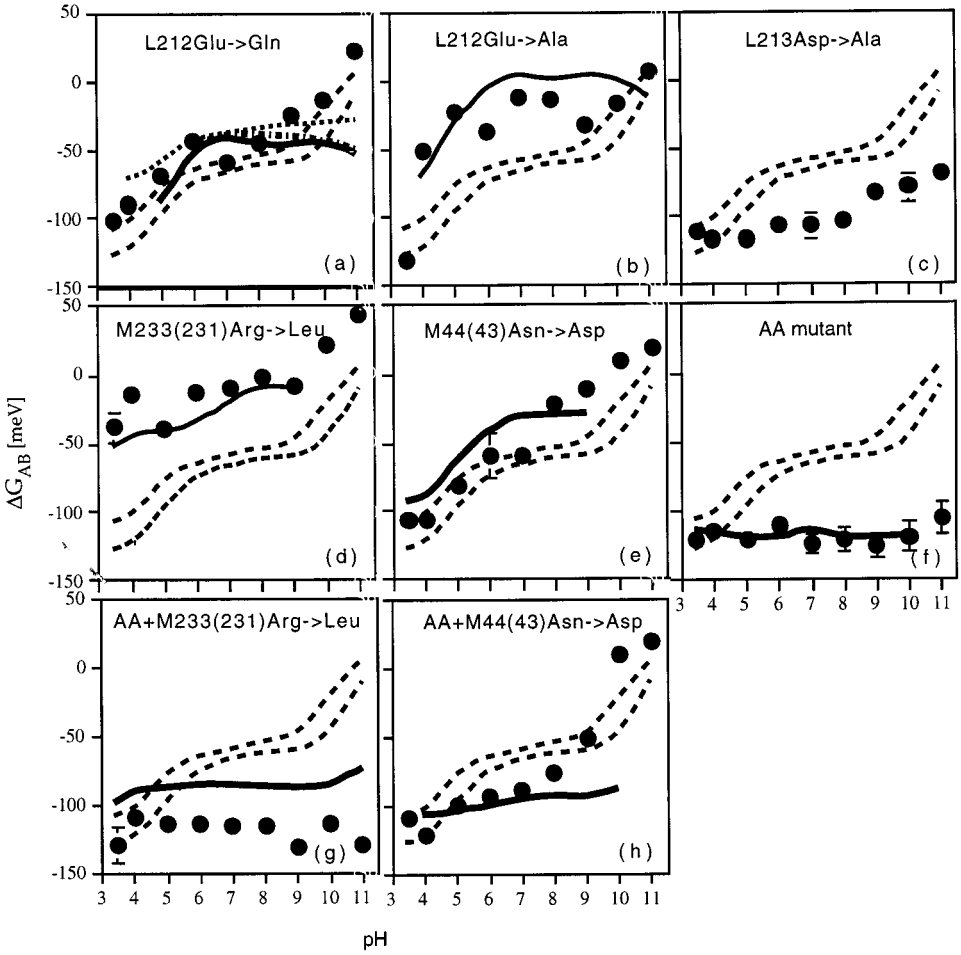

FIGURE 3: pH titration of thefree energy of the electron transfer from Q_A^- to Q_B. Calculated free energies (●). The envelope of the experimental data from WT RCs from Figure 1 is given by the two dashed lines. Experimental data for mutants are shown by the other lines. (a)L212Glu → Gln mutant. The solid line represents the experimental data from ref *35* (*Rb. caplulatus* RCs), dotted line from ref *33*, and dash−dotted line from ref *37* (*Rb sphaeroides* RCs). (b)L212Glu → Ala. Experimental data are shown by the bold line. (c) L213Asp → Ala. (d) M231(233)Arg → Leu mutant. (e) The M43(44)Asn → Asp mutant. (f) L212Glu−L213Asp → Ala−Ala (AA) mutant. (g) AA + M231(233)Arg→Leu revertant RC. (h) AA + M43(44)Asn→Asp revertant RC. Experimental data for b−h from ref *31* (*Rb. caplulatus* RCs).

ionized and L212Glu is partially ionized in the ground state at pH 7. The net charge of the cluster of three residues is −1.25 in WT and −1.15 in mutant RCs.

The electron transfer from Q_A^- to Q_B is calculated to be more favorable in the mutant than in WT RCs. Residue ionization and conformation in the $Q_AQ_B^-$ state are little changed on removing Asp which is neutral when Q_B is reduced. In contrast, in the $Q_A^-Q_B$ state, L213Asp is fully ionized. Thus, removing L213Asp changes the ionization of surrounding residues in the ground and $Q_A^-Q_B$ but not the $Q_AQ_B^-$ states. Thus, the calculated $-\Delta G_{AB}$ notably increases in the mutant mostly because the L213Asp → Ala mutation destabilizes the reactant $Q_A^-Q_B$ state, rather than stabilizes the product, $Q_AQ_B^-$ state. In the $Q_A^-Q_B$ state, the carboxyl group of $L213Asp^-$ makes a strong hydrogen bond to the hydroxyl of L223Ser (*10*), which is lost in the mutant. The calculations suggest that the loss of the hydrogen bond destabilizes the $Q_A^-Q_B$ state in the mutant compared to the WT. In the $Q_AQ_B^-$ state, the L223Ser makes a hydrogen bond to Q_B^-, which is not affected by the removal of L213Asp.

Table 2 provides the changes calculated to occur upon formation of the $Q_A^-Q_B$ and $Q_AQ_B^-$ states. L212Glu binds $0.15H^+$/RC to become fully protonated in the $Q_AQ_B^-$ state. The pH independence of ΔG_{AB} at physiological pHs shows that there is no proton uptake from solution.

M231(233)Arg → Leu Mutant. M231(233)Arg → Leu mutation was identified in a *Rb. capsulatus* photocompetent phenotypic revertant derived from the photosynthetically incompetent L212Glu-L213Asp → Ala−Ala double mutant strain. Experimentally, at pH 7, the single M231Arg → Leu mutation results in a 40 meV less favorable $-\Delta G_{AB}$ compared to the WT RCs. At pH 7, in the mutant, $-\Delta G_{AB}$ is measured to be 20 meV and calculated to be 15 meV (Figure 3d). At high pH, the calculations suggest that $-\Delta G_{AB}$ should have a similar pH dependence to that found in WT RCs.

In the previous calculations with WT RCs, M231(233)-Arg is fully ionized in the ground, $Q_A^-Q_B$, and $Q_AQ_B^-$ states as are the nearby H232(230)Glu and H125(122)Glu. M231-(233)Arg forms salt bridges with H232(230)Glu and H125-(122)Glu, keeping them ionized even at low pH. Thus, this cluster has a net charge of −1. When the Arg is changed to Leu, in the ground state, H232(230)Glu binds a proton while H125(122)Glu remains mostly ionized (Table 1). Thus, the net charge on the cluster is unchanged although the charge distribution varies (*44*). This is similar to the behavior found

Table 1: Comparison of Ionization and Conformation States Calculated for Each Mutant and for the Native Structure[a]

mutant	ionization differences $z_i^{native} - z_i^{mutant}$ (pH 7)	residues undergoing conformation changes (pH 7)	$\Delta\Delta G_{AB} = \Delta G_{AB}^{native} - \Delta G_{AB}^{mutant}$ (pH 7) (meV)		pH dependence of ΔG_{AB}					
			experiment	theory	experiment			theory		
					L	I	H	L	I	H
wild-type			0 (by definition)	0 (by definition)	+	0	+	+	0	+
L212Gln	none	none	−20	− 25	+	0	0	+	0	+
L212Ala	none	none	−60	−70	+	0	≈−	+	0	≈+
L213Ala	L210Asp, **−0.75** L212Glu, **−0.15**	H130Lys L217Arg L223Ser M43(44)Asn	ND	+25	ND	ND	ND	0	0	≈+
M233 (231)Leu	H232(230)Glu, +1.0	none	−40	−70	0	0	ND	0	0	+
M43(44)Asp	L210Asp, **−0.15** L213Asp, +0.60 M43(44)Asp, **−0.45**	L217Arg L223Ser	−30	−25	+	0	ND	+	0	+
AA	L210Asp, **−0.75**	H130Lys L217Arg L223Ser M43(44)Asn	+55	+40	0	0	0	0	0	0
AA+ M233 (231)Leu	H125(122)Glu, +0.15 H232(230)Glu, +1.0 L210Asp, **−0.75**	L217Arg L223Ser M43(44)Asn	+25	+30	0	0	0	0	0	0
AA+ M43(44)Asp	L210Asp, **−0.55** M43(44)Asp, **-0.45**	H130Lys L217Arg L223Ser	+35	+5	0	0	0	0	0	+

[a] Bold values: residue charge increases by acid loosing a proton or base gaining a proton. The pH dependence of ΔG_{AB} is given in the three regions discussed: low (L), intermediate (I), and high (H) pH regions. (0) No pH dependence; (−) reaction more favorable with increasing pH; (+) reaction less favorable with increasing pH; (≈) weak pH dependence, (ND) not determined.

in the L213Ala mutant where removing a negative charge on one acid allows two nearby, protonated acids to become partially ionized. M231(233)Arg^+ and H232(230)Glu^- are 2.7 Å apart lying about 15 Å from Q_B. This ion pair will look like a dipole from the vantage point of the distant Q_B. Thus, removing M231(233)Arg can be seen as removing a dipole not a charge.

M231(233)Arg, H125(122)Glu, H232(230)Glu, and M234-(236)Glu do not change conformation or ionization states on the electron transfer from Q_A^- to Q_B in the WT RCs (Table 2). Removing the charge of M231(233)Arg plus H232(230)Glu changes $-\Delta G_{AB}$ largely because of the asymmetry of the interactions of Arg and Glu with Q_B^-. The interaction energy between M231(233)Arg^+ and Q_B^- is 70 meV, while the interaction of H232(230)Glu^- and Q_B^- is only +40 meV. Thus, the removing the ion pair M231(233)-Arg−H232(230)Glu destabilizes the $Q_AQ_B^-$ state. In addition, on electron transfer from Q_A^- to Q_B, some proton transfer from H232(230)Glu to H125(122)Glu occurs, which will also influence the $-\Delta G_{AB}$.

M43(44)Asn → Asp Mutant. The M43Asn → Asp mutation in *Rb. capsulatus* was found in a photocompetent phenotypic revertant derived from the photosynthetically incompetent L212Glu−L213Asp → Ala−Ala double mutant strain. Wild-type *Rbs. viridis* RCs have an Asp at the M44 position and an Asn at L213. A difference of ∼30 meV was observed between the $-\Delta G_{AB}$ measured in the M43Asn → Asp single mutant and WT RCs (Figure 3e) (*44*). The calculations show a similar $\Delta\Delta G_{AB}$ of ∼25 meV. The calculated and experimental pH dependence of $-\Delta G_{AB}$ are similar in the low and intermediate pH ranges (Figure 3e). There are no measurements at high pH.

In the M43(44)Asn → Asp mutant, the calculations suggest that the introduced Asp is 45% ionized and that L213Asp and L210Asp are, respectively, 60% less and 15% more ionized than in the native structure (Table 1). Therefore, the introduction of the Asp near the preexisting cluster results in a redistribution of charge, but little change in the total RC charge.

The M43(44)Asn → Asp mutation replaces a dipole by a potentially negatively charged group. The group has a small fractional charge in the $Q_A^-Q_B$ state and is fully protonated in the $Q_AQ_B^-$ state. In the $Q_A^-Q_B$ state, in the mutant, the calculations show an average charge of −0.8 on L213Asp (−1 in the WT), −0.15 on L210Asp (0 in the WT), and −0.15 on M43(44)Asp. In the mutant, there is a redistribution of part of the negative charge on L213Asp further from Q_A^-. In the $Q_AQ_B^-$ state, M43(44)Asp is calculated to be fully protonated. Since M43(44)Asn and the protonated M43(44)-Asp have practically the same pairwise interaction energies with the rest of the protein, the mutation is expected to have little effect on the free energy level of the $Q_AQ_B^-$ state. Therefore, the less favorable $-\Delta G_{AB}$ value measured in experiments appears to result from the stabilization of the $Q_A^-Q_B$ state in the mutant.

The difference in ionization and conformation changes in WT RCs and in the mutant that occur on the electron transfer is shown in Table 2. The proton uptake is now significant at pH 7 resulting in pH dependence of the $-\Delta G_{AB}$. As in WT RCs, a fraction of a proton is transferred from the L210Asp to the coupled acids L213Asp−M44Asp (Table 2).

L212Glu−L213Asp → Ala−Ala Double Mutant (AA). The L212Glu−L213Asp → Ala−Ala double mutation is calculated to stabilize the $Q_AQ_B^-$ state relative to the $Q_A^-Q_B$ state

Table 2: Conformation and Ionization Changes Calculated for the First Electron Transfer for Each of the Mutants and for Native RCs

	$PQ_AQ_B \rightarrow P^+Q_A^-Q_B$		$P^+Q_A^-Q_B \rightarrow P^+Q_AQ_B^-$	
mutant	ionization	conformation	ionization	conformation
native	none	M43(44)Asn, M232Glu	L210Asp, **−0.70** L213Asp, +0.90	L217Arg, H130Lys, L223Ser, M43(44)Asn
L212Gln	none	M43(44)Asn, M232Glu	L210Asp, **−0.70** L213Asp, +0.90	L217Arg, H130Lys, L223Ser, M43(44)Asn
L212Ala	none	M43(44)Asn, M232Glu	L210Asp, **−0.60** L213Asp, +0.90	L217Arg, H130Lys, L223Ser, M43(44)Asn
L213Ala	none	L212Glu, L217Arg, L223Ser, M232Glu	L212Glu, +0.15	L212Glu, L222Tyr, L217Arg, L223Ser, M232Glu
M231(233) Leu	M234(236)Glu, **−0.40** H125(122)Glu, +0.35	L212Glu, M232Glu, M43(44)Asn	L210Asp, **−0.40** L213Asp, +0.90	L217Arg, H130Lys, L223Ser, M43(44)Asn
M43(44)Asp	L210Asp, +0.15 L213Asp, −0.50 M43(44)Asp, +0.30	L217Arg	L210Asp, **−0.35** L213Asp, +0.70 M43(44)Asp, +0.15	L217Arg
AA	none	L217Arg, L223Ser, M43(44)Asn, M232Glu	none	L217Arg, L222Tyr, L223Ser, M43(44)Asn
AA + M233 (231)L	H125(122)Glu, 0.85 L210Asp, −0.10 M234(236)Glu, −0.80	L217Arg, L223Ser, M43(44)Asn, M232Glu, H130Lys	none	L217Arg, L222Tyr, L223Ser, M43(44)Asn, M232Glu
AA + M44 (43)D	L210Asp, **−0.20** M43(44)Asp, −0.40	L217Arg, M232Glu, H130Lys	none	L217Arg, L222Tyr, L223Ser

[a] Only changes larger than 10% (with respect to the initial state) are shown. If no numerical value is given, residue changes conformation and not ionization state. Numerical values show the change in average residue ionization in the Boltzmann distribution of accepted microstates. Bold values indicate an increase in fractional ionization as acids loose a proton or bases bind a proton.

by about 40 meV, in good agreement with the measured value of 55 meV (*56*) (Figure 3f, Table 1). However, in this mutant, the rate of charge recombination is so slow that it may underestimate the $-\Delta G_{AB}$ value (*59*). Neither calculated nor measured $-\Delta G_{AB}$ shows pH dependence.

The major difference in ionization states between WT RCs and the mutant was found to be at L210Asp. In the absence of L213 and L212, now L210 is fully ionized in all states at physiological pHs (Table 1). The calculation of the distribution of the conformer occupancies shows that, at pH 7, ionization and conformation changes for the AA mutant are the same as those calculated for the L213Asp → Ala single mutant. The only difference was calculated at high pH, where L212Glu begins to titrate in the L213Asp → Ala mutant. In the absence of both L212Glu and L213Asp, no protons are bound from the solution on electron transfer from Q_A^- to Q_B (pH 6−11) (Table 2).

AA + M231(233)Arg → Leu Revertant. In this revertant RC, $-\Delta G_{AB}$ was measured to be ∼30 meV smaller than in the AA double mutant (*56*) but was computed to be decreased only by 10 meV. In both cases, a reasonably good agreement is observed between the pH independence of the experimental and calculated $-\Delta G_{AB}$ curves (Figure 3g). However, the experimental and calculated $-\Delta G_{AB}$ values differ by about 20−30 meV at all pHs. This is clearly the least accurate fit of the experimental data in the intermediate pH region. Possible explanations for this discrepancy is the significant rearrangement of charged groups near to the M233(231) observed experimentally (*61*), which are not embedded into the model.

The calculations show that the mutations present in this phenotypic revertant RC change the energy of both $Q_A^-Q_B$ and $Q_A Q_B^-$ states compared to the WT RCs. As mentioned above, the L213Asp → Ala destabilizes the $Q_A^-Q_B$ state by removing the hydrogen bond to L223Ser, while the $Q_AQ_B^-$ state is destabilized by replacing M231(233)Arg by Leu and by neutralization of the H232(230)Glu counter charge. Bringing both effects together in the AA + M231-(233)Arg → Leu revertant RC, yields ΔG_{AB} similar to WT RCs (Table 1).

The analysis of the distribution of the ionization and conformation states shows that there are several major

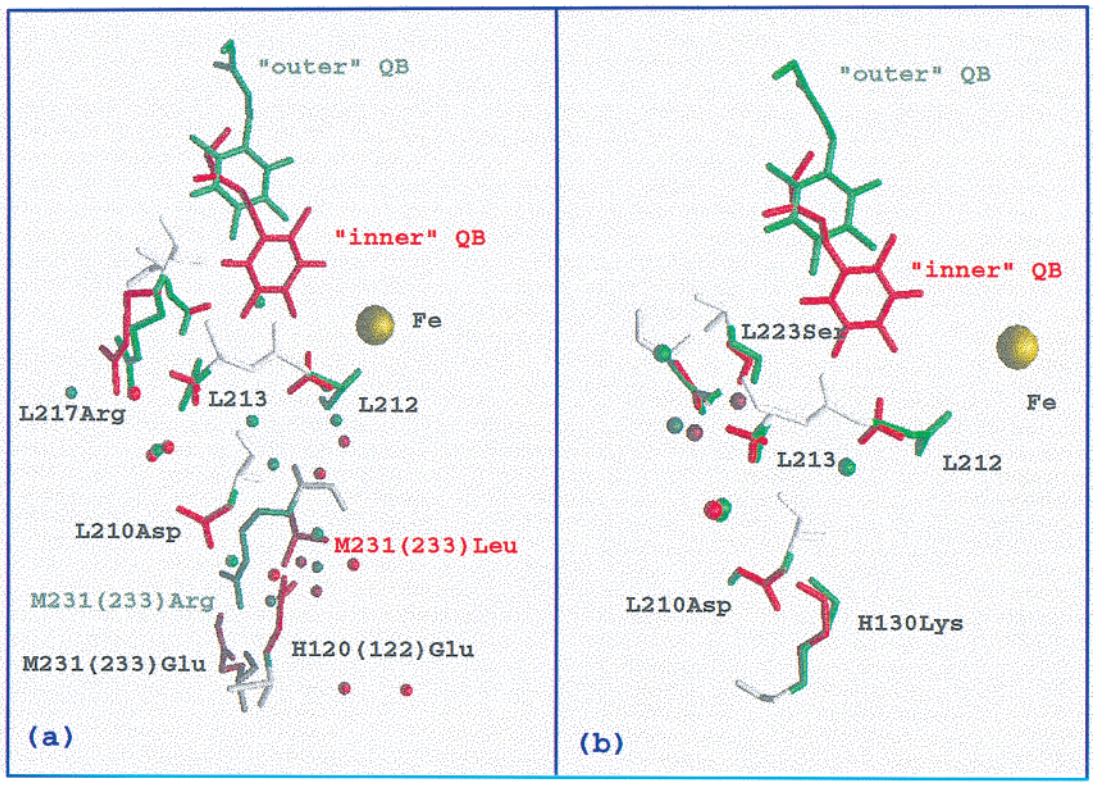

FIGURE 4: Calculated conformational and ionization differences between the native structure (*9*) and the mutant in the ground state at pH 7. The highly occupied conformers in the native structure are shown in green and highly occupied conformers in the mutant are shown in red. Waters affected by the mutation are shown as balls. These changes are in Table 2. (a) The L212Glu−L213Asp−M231(233)Arg → Ala-Ala-Leu [AA + M231(233)RL] revertant RC. (b) The L212Glu−L213Asp−M43(44)Asn → Ala-Ala-Asp [AA + M43(44)ND] revertant RC.

differences in the ground state in this triple mutant (Table 1). The changes are almost additive and are approximately the sum of those calculated for AA and M231(233)Arg → Leu mutant. However, a small proton redistribution was calculated between H122Glu and M236Glu, that is not seen in either the single or double (AA) mutants. The most occupied conformers calculated for the WT and AA + M231(233)Arg → Leu revertant RCs in the ground state, at pH 7 are shown in Figure 5a. Most of the changes are associated with the salt bridge H125(122)Glu−M231(233)-Arg−H232(230)Glu, which now is broken because of the removal of M231(233)Arg. In addition, the absence of L213Asp causes reorientation of the side chain of L217Arg.

No ionization changes are calculated to occur on the Q_A^- to Q_B electron transfer (Table 2). Upon the formation of either semiquinone, the largest conformation changes are calculated for L223Ser, M43(44)Asn, and L217Arg. In addition to these groups, a large number of waters change their orientation and position. Conformers on the diagonal do not change occupancy. Those on the right of the diagonal are less probable in RCs with Q_B^-, while points on the left are more populated in the $Q_AQ_B^-$ state. The deviation from the diagonal is minimal near conformer probabilities of 0 and 1. Most off-diagonal elements are residues with several conformers with similar occupancy and thus comparable energies. The protein undergoes many small conformation and ionization changes upon quinone reduction, each of them contributing to the reaction free energy in addition to significant changes in a few residues.

AA + M43(44)Asn → Asp Revertant. At pH 7, the $-\Delta G_{AB}$ calculated for this revertant is about 35 meV less favorable than in the AA RC. Experimentally, a value of $\Delta\Delta G_{AB}$ 20 meV was determined (*31*). Experimentally $-\Delta G_{AB}$ shows little pH dependence, becoming slightly less favorable from pH 4 to 10. The calculated values of $-\Delta G_{AB}$ decrease sharply above pH 7 (Figure 3h), predicting that reaction becomes unfavorable above pH 10.

The effects of the three different mutations measured in the AA + M43(44)Asn → Asp revertant RC are roughly additive (*44*). Thus, the AA mutations make $-\Delta G_{AB}$ more favorable, while M43(44)Asn → Asp mutation makes it less favorable. The result of these two opposing effects is that the $-\Delta G_{AB}$ in AA + M43(44)Asn → Asp revertant is close to that found in WT RCs (Table 1).

Two groups become charged in the absence of L213Asp. In the mutant, L210Asp takes 55% the charge while M43-(44)Asp takes 45%. Thus, the net charge remains unchanged but it is distributed differently compared to WT RCs. Conformation and ionization changes in the AA + M43-(44)Asn → Asp mutant are shown in Figure 5b. This triple mutation causes significant side-chain rearrangement and protonation changes. Since, L213Asp is fully ionized in WT RCs in the ground and the $Q_A^-Q_B$ states, replacing it with Ala changes significantly the free-energy level of the $Q_A^-Q_B$ state. Additionally, replacing M43(44)Asn by Asp, which is calculated to be partially ionized in the $Q_A^-Q_B$ state in the mutant, also affects the energy of this state. Thus, the AA mutations destabilize the $Q_A^-Q_B$ state and the M43(44)Asn → Asp substitution stabilizes it, by providing a residue that accepts 45% of the charge of the missing L213Asp. The overall effect is an almost WT $-\Delta G_{AB}$ value in the AA + M43(44)Asn → Asp revertant RC.

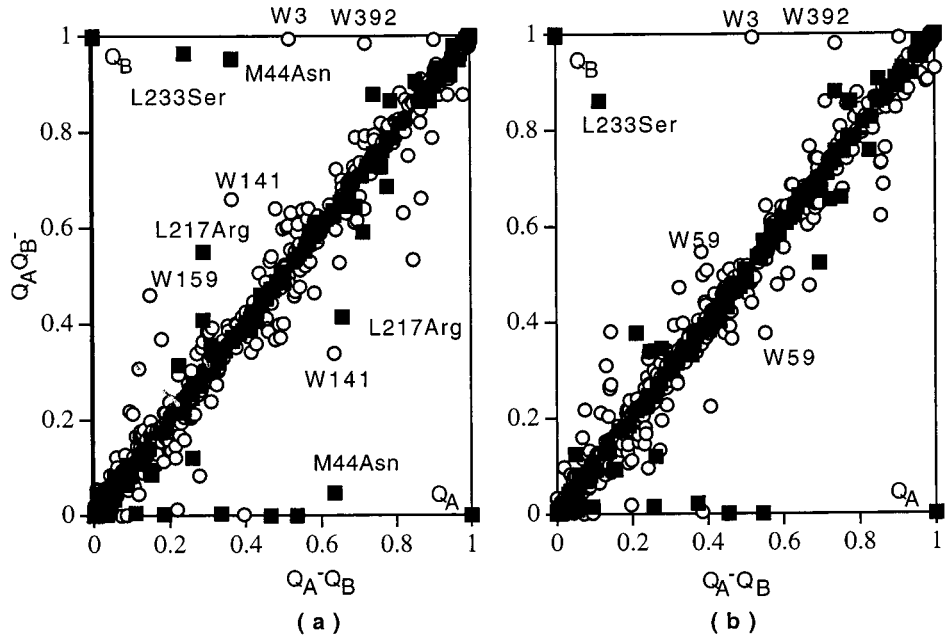

FIGURE 5: Ionization and conformation changes upon the first electron transfer from Q_A^- to Q_B. Solid squares represent changes in occupancy of protein conformers and open circles represent water conformers. The points on the diagonal do not undergo conformation changes while points to the right of the diagonal lower their occupancy and points to the lest increase their conformer occupancy upon quinone reduction. (a) The L212Glu−L213Asp−M231(233)Arg → Ala-Ala-Leu [AA + M231(233)L] revertant RC. (b) The L212Glu−L213Asp−M43(44)-Asn → Ala-Ala-Asp [AA + M43(44)D] revertant RC.

Table 3: Water Conformational Changes[a]

mutant	water occupancy changes from WT	water occupancy changes $P^+ Q_A^- Q_B \rightarrow P^+ Q_A Q_B^-$ [b]
L212EQ	slight change in P1 channel (largest change, W5)	all channels but (P2, P3 are more active)
L212EA	slight change in P1 channel (largest change, W5)	all channels but (P2, P3 are more active)
L213DE	significant changes in P2 and P3 channels only	all channels but P1 is more active
M231(233)RL	significant changes in P1 and P2 channel	channel P1 is more active
M43(44)ND	significant changes in P2 channel only	all channels but most active channel is P1
AA	most of the changes within P2 and P3 channels (W6, 200,201) and P1 (W5)	channel P1 is more active
AA + M231(233)RL	significant changes in P1 and P2 channel	channel P1 is more active
AA + M43(44)ND	significant changes in P2 and P3 channels	channel P1 is more active

[a] Second column provides changes of water occupancy in the ground state in given mutant compared to WT RCs. [b] Third column compares changes in water occupancy on the first electron transfer in mutant and WT RCs. Water numbering from ref *9*.

The mutations do not affect significantly the free energy of the $Q_AQ_B^-$ state compared to the WT. In the WT, L212Glu and L213Asp were calculated to be protonated (*23*, *25*, *26*). In the AA + M43(44)Asn → Asp revertant RC, M43(44)-Asp is calculated to be protonated in the $Q_AQ_B^-$ state. Therefore, the substitution of these three groups causes only small changes in the free-energy level of the $Q_AQ_B^-$ state compared to WT RCs.

Figure 6b illustrates the calculated ionization and conformation changes occurring upon electron transfer from Q_A^- to Q_B in the RCs from the AA + M43(44)Asn → Asp strain. Several groups undergo conformational changes, but no ionization changes were calculated (Table 2). Except for L223Ser and L217Arg, all other significant changes are associated with waters.

Water Molecules. In numerical calculations, waters were found to play a significant role in determining the $-\Delta G_{AB}$ (*25*). The number of water molecules identified by the X-ray structures is quite large (*9*, *10*, *12*). There is a growing consensus that they can be grouped into several distinct channels in the different X-ray structures. Water molecules are arranged as a channel leading to Q_B, perpendicular to the membrane [called "P1" (*12*, *62*, *63*)]. Two other channels lead to Q_B running parallel to the membrane ["P2" and "P3"-(*62*, *63*)].

The occupancies of the water sites previously calculated in WT RCs (*25*) are compared to those calculated here in the mutant RCs. Waters in the mutants were found to have about 50% average occupancy, similar to that found in the WT RCs.

Combining the waters in the 1AIG and 1AIJ RC structures 126 water sites were identified. No extra waters were added on introducing the various mutations. However, most waters identified in the crystal structure were allowed to have a large number of orientations and positions. Waters also have a conformation outside the protein. Thus, the initially proposed waters can change their occupancies due to a given mutation mimicking water bindings, translation, and rotation within the site.

In the ground state, the water distribution calculated for each mutant was compared to the water occupancy of the WT RCs. The results are shown in Table 3. The L212Gln and L212Ala substitutions do not cause significant differences in water occupancy compared to the WT RCs. There

are only small changes in water distribution within the P1 channel in the vicinity of Q_B. The picture is quite different for the L213Asp → Ala mutant (Table 3), where most of the changes are within the P2 and P3 channels. Most of the changes in M43(44)Asn → Asp mutant are also associated with waters forming the P2 and P3 channels. The AA double mutant has the same effect as the L213Asp → Ala single mutant, because the L212Ala substitution does not cause significant water rearrangement. The AA + M231(233)Arg → Leu revertant RC has sites of mutations near both the P1 [M231(233)] and the P2 and P3 (L213) channels. As a result, waters that change position are found in both channels (Table 3 and Figure 5a). Finally, the mutations present in the AA + M43(44)Asn → Asp revertant RC mostly cause rearrangements within the P2 and P3 channels (Table 3 and Figure 5b).

Most of the changes associated with the first electron transfer in the L212Glu → Gln and L212Glu → Ala mutants are quite similar to the WT and involve members of all three water channels (Table 3), with most changes associated with the P2 and P3 channels. Replacing either L213Asp by Ala or M43(44)Asn by Asp yields large changes in the P1 channel (Table 3). This is also true for the AA double mutant and for the revertants.

DISCUSSION

The free energy of the electron transfer from Q_A^- and Q_B ($-\Delta G_{AB}$) has been calculated in eight mutants where ionizable amino acids have been added or removed. Substitutions of residues at sites close to Q_B (L212Glu, L213Asp) as well as substitutions at more distant sites that were identified in phenotypic revertants [L231(233)Arg, M43(44) Asn] were considered. Previous calculations on WT RC fit experimental $-\Delta G_{AB}$ (*25*) with an error of ∼20 meV (pH 5−11). A detailed atomic model for the protein which allows motions of Q_B, side chains, waters, and hydroxyls during the energy calculations was used (*25*). The same WT structure, method, and parameters were used here to calculate the effects of the different mutations whose side chains replaced the native one. Previous experiments with RCs from the L212Glu−L213Asp → Ala−Ala double mutant and the two phenotypic revertants, in which the M43(44)Asn → Asp and M231(233)Arg → Leu mutations compensate for the lack of L212Glu and L213Asp, considered the energetics and the dynamics of the electron and proton-transfer processes (*20*). However, these experiments could not identify the ionization states or motions of side chains and water molecules that could be changed in mutant RCs. The calculations represented here provide information that helps understand the changes caused by each of the mutations.

Each mutation adds or subtracts an ionizable group from the protein. The formal pairwise interactions of these residues, if charged, with Q_B^- range from 330 meV for L212Glu and 300 meV for L213Asp to −70 meV for M231-(233)Arg. However, measured and calculated $\Delta\Delta G_{AB}$s in the mutants vary by less than ±60 meV. Two mechanisms play a role in reducing the $\Delta\Delta G_{AB}$. First, with exception of the more distant M231(233)Arg, all other residues subject to mutation are neutral in the $Q_AQ_B^-$ state. So, these large pairwise interactions with Q_B^- never contribute to $-\Delta G_{AB}$. In addition, when the group is ionized in the $Q_A^-Q_B$ [L213Asp, M43(44)Asp] or in both $Q_A^-Q_B$ and $Q_AQ_B^-$ states [M231(233)Arg), its addition or subtraction causes changes in the ionization within a particular cluster of strongly interacting groups. Ionization changes within the cluster keep the net charge unchanged, reducing the effect of the mutation. Each new protein charge distribution does change ΔG_{AB} compared to WT RCs by a modest, but easily measurable amount. However, the change would be much larger without protein rearrangement that maintains the net charge of the protein. For example, the substitution of L213Asp, which is calculated to be ionized in the native structure in the ground and the $Q_A^-Q_B$ states, by a nontitratable residue causes ionization of L210Asp, keeping the charge within the Q_B pocket close to what it is in the native structure. For the M231(233)Arg → Leu mutant, removal of the positive charge is compensated by neutralizing H232(230)Glu in the ground and $Q_A^-Q_B$ states and by additional charge redistribution in the $Q_AQ_B^-$ states again keeping the charge of the cluster practically constant.

In each mutant, the change in $-\Delta G_{AB}$ can be caused by changes in the free-energy levels of either of the semiquinone states. The effect of a given mutation depends on the initial role that the native side chain has on the free-energy levels of the $Q_A^-Q_B$ and $Q_AQ_B^-$ states rather than its position relative to Q_A or Q_B. Thus, several mutations have the largest effect on the $Q_A^-Q_B$ state despite the residue being close to Q_B. For example, initial analysis of the L213Asp → Ala mutant proposed that the more favorable $-\Delta G_{AB}$ resulted from removing a charge 4 Å away from Q_B. However, L213Asp does not contribute significantly to the energy of the $Q_AQ_B^-$ state, because it is fully protonated in this state. Rather, it makes a significant contribution to the free energy of the Q_B pocket in the $Q_A^-Q_B$ state (*23*, *34*, *35*) (Figure 3b).

Triple-mutant, revertant RCs show larger ionization and conformational changes, which again maintain the net charge of the system. The AA + M43(44)Asn → Asp strain produces smaller ionization changes than AA + M231(233)-Arg → Leu, because one acid (L213Asp) is removed while another is added [M43(44)Asp]. The negative charge on L213Asp in ground and $Q_A^-Q_B$ states is now distributed between M43(44)Asp and L210Asp. The smaller ionization changes in AA + M43(44)Asn → Asp compared to the AA + M231(233)Arg → Leu RCs are caused by the difference in the third site of mutation. M43(44) site is within AA cluster of residues, while M231(233) is relatively far away from this cluster. Thus, the AA + M43(44)Asn → Asp revertant changes residues within a single cluster (AA cluster) while AA + M231(233)Arg → Leu changes residues within two clusters causing larger ionization and conformation changes.

The electron transfer in the mutants which replace L213Asp with a neutral residues without introducing an Asp at M43(44) lack pH dependence at high pH in experiment and calculation. As seen in previous calculations on WT RCs (*23*, *25*, *26*), Asp L213 is ionized in the $Q_A^-Q_B$ state and must bind a proton when the electron is transferred to Q_B. This proton is primarily donated by L210Asp at physiological pH. At high pH, changes in ionization states of other residues contribute some of the proton needed by L213Asp, but some RCs in the ensemble must bind a proton from solution. Removing L213Asp thus removes the requirement for proton

binding, diminishing the pH dependence of the reaction. M43(44)Asn lies near Q_B. When an Asp is substituted at this site, it is partially ionized in the $Q_A^-Q_B$ state and neutral in the $Q_AQ_B^-$ state. This restores some of the pH dependence of the reaction $-\Delta G_{AB}$ at high pH.

The calculations fail to capture the pH independence in the high pH region of the L212Glu → Gln and L212Glu → Ala mutant RCs. When a site is reduced within a protein, the product state can be stabilized by protein rearrangement or by proton binding. These MCCE calculations, with a limited number of side-chain conformers, may lack sufficient conformational flexibility to capture motions available in the protein that stabilize the $Q_AQ_B^-$ state without proton uptake. In addition, as described previously (*25*) proton uptake can occur even at distant sites at pHs near a residue's p*K*. Many residues titrate above pH 9. Small errors in their calculated p*K*s can therefore lead to significant errors in proton uptake at high pH.

The calculations also differ from experiment in the analysis of the AA + M231(233)Arg → Leu mutant. In the calculations, the reaction is more favorable than measured. What is notable is that the experimentally determined $\Delta\Delta G_{AB}$ is rather close to the numerical sum of the $\Delta\Delta G_{AB}$ of the AA mutant, which destabilizes the $Q_A^-Q_B$ state and the M231(233)Arg → Leu single mutant which stabilizes the $Q_AQ_B^-$ state. In contrast, the calculations show changes in the triple mutant that are not found in either parent single or double mutants (see Table 2). It may be that changes in the protein, not captured in the model isolate the L212, L210, and L213 cluster (AA) from the M231(233)Arg, H232(230)-Glu, and H125(122)Glu cluster resulting in the observed independence of the effects of AA and Arg mutations.

Both mutations accelerate proton transfer by more than 50-fold compared to the AA mutant (*31*) and were originally suggested to occur near proton transport channels involving water molecules (*56*) The high-resolution structures of the *Rb. sphaeroides* RC (*9*, *12*, *62*, *63*) show that the M43(44) and M231(233) sites are near specific water channels. The numerical calculations performed for the WT RC (*25*) showed that the electron transfer from Q_A^- to Q_B states does involve changes in the occupancy of conformers of water molecules in or close to these channels. In the different genetically modified RCs, the electron transfer appears to be accompanied by significant modifications of the positions and/or orientations of water molecules in the various water channels. Such a possible coupling between the motions of water molecules along the channels and the electron transfer process has recently been suggested (*64*).

REFERENCES

1. Li, J., Gilroy, D., Tiede, D. M., and Gunner, M. R. (1998) *Biochemistry 37*, 2818−2829.
2. Tiede, D. M., Vazquez, J., Cordova, J., and Marone, A. P. (1996) *Biochemistry 35*, 10763−10775.
3. Graige, M. S., Feher, G., and Okamura, M. Y. (1998) *Proc. Natl. Acad. Sci. U.S.A. 95*, 11679−11684.
4. Lavergne, J., Matthews, C., and Ginet, N. (1999) *Biochemistry 38*, 4542−4552.
5. Maroti, P., and Wraight, C. A. (1988) *Biochim. Biophys. Acta 934*, 329−347.
6. McPherson, P. H., Okamura, M. Y., and Feher, G. (1988) *Biochim. Biophys. Acta 934*, 348−368.
7. Wraight, C. A. (1979) *Photochem. Photobiol. 30*, 767−776.
8. Wraight, C. A. (1998) in *Proceedings of the XIth International Photosynthesis Congress* (Garab, G., Ed.) pp 693−698, Kluwer, Dordrecht.
9. Stowell, M. H. B., McPhillips, T. M., Rees, D. C., Soltis, S. M., Abresch, E., and Feher, G. (1997) *Science 276*, 812−816.
10. Lancaster, R., and Michel, H. (1997) *Structure 5*, 1339−1359.
11. Deisenhofer, J., and Michel, H. (1991) *Annu. Rev. Biophys. Chem. 20*, 247−266.
12. Ermler, U., Fritzsch, G., Buchanan, S. K., and Michel, H. (1994) *Structure 2*, 925−936.
13. Deisenhofer, J., and Michel, H. (1989) *EMBO J. 8*, 2149−2170.
14. Williams, J. C., Steiner, L. A., and Feher, G. (1986) *Proteins 1*, 312−325.
15. El-Kabbani, O., Chang, C.-H., Tiede, D., Norris, J., and Schiffer, M. (1990) *Biochemistry 30*, 5361−5369.
16. Foloppe, N., Ferrand, M., Breton, J., and Smith, J. C. (1995) *Proteins: Struct., Funct., Genet. 22*, 226−244.
17. Gunner, M. R. (1991) *Curr. Top. Bioenerg. 16*, 319−367.
18. Okamura, M. Y., and Feher, G. (1992) *Annu. Rev. Biochem. 61*, 861−896.
19. Takahashi, E., and Wraight, C. A. (1994) *Adv. Mol. Cell Biol. 10*, 197−251.
20. Sebban, P., Maroti, P., and Hanson, D. K. (1995) *Biochimie 77*, 677−694.
21. Blankenship, R. E., Madigan, M. T., and Bauer, C. E. (1995) *Anoxygenic Photosynthetic Bacteria*, Vol. 2, Kluwer Academic Publishers.
22. Sham, Y. Y., Muegge, I., and Warshel, A. (1999) *Proteins: Struct., Funct., Genet. 36*, 484−500.
23. Beroza, P., Fredkin, D. R., Okamura, M. Y., and Feher, R. (1995) *Biophys. J. 68*, 2233−2250.
24. Lancaster, C. R. D., Michel, H., Honig, B., and Gunner, M. R. (1996) *Biophys. J. 70*, 2469−2492.
25. Alexov, E., and Gunner, M. (1999) *Biochemistry 38*, 8253−8270.
26. Gunner, M. R., and Honig, B. (1992) in *The Photosynthetic Bacterial Reaction Center: Structure, Spectroscopy and Dynamics II* (Breton, J., and Vermeglio, A., Eds.) pp 403−410, Plenum, New York.
27. Rabenstein, B., Ullmann, G. M., and Knapp, E.-W. (1998) *Eur. Biophys. J. 27*, 626−637.
28. Baptista, A. M., Martel, P. J., and Peterson, S. B. (1997) *Proteins: Struct., Funct., Genet. 27*, 523−544.
29. Spassov, V. Z., and Bashford, D. (1999) *J. Comput. Chem. 20*, 1091−1111.
30. Alexov, E. G., and Gunner, M. R. (1997) *Biophys. J. 72*, 2075−2093.
31. Maroti, P., Hanson, D. K., Baciou, L., Schiffer, M., and Sebban, P. (1994) *Proc. Natl. Acac. Sci. USA 91*, 5617−5621.
32. Paddock, M. L., Feher, G., and Okamura, M. Y. (1997) *Biochemistry 36*, 14238−14249.
33. Takahashi, E., and Wraight, C. A. (1992) *Biochemistry 31*, 855−866.
34. Takahashi, E., and Wraight, C. A. (1990) *Biochim. Biophys. Acta 1020*, 107−111.
35. Paddock, M. L., Rongey, S. H., McPherson, P. H., Juth, A., Feher, G., and Okamura, M. Y. (1994) *Biochemistry 33*, 734−745.
36. McPherson, P. H., Schonfeld, M., Paddock, M. L., Okamura, M. Y., and Feher, G. (1994) *Biochemistry 33*, 1181−1193.
37. Paddock, M. L., Rongey, S. H., Feher, G., and Okamura, M. Y. (1989) *Proc. Natl. Acad. Sci. U.S.A. 86*, 6602−6606.
38. Miksovska, J., Kalman, L., Schiffer, M., Maroti, P., Sebban, P., and Hanson, K. (1997) *Biochemistry 36*, 12216−12226.
39. Hienerwadel, R., Grzybek, S., Fogel, C., Kreutz, W., Okamura, M. Y., Paddock, M. L., and Breton, J. (1995) *Biochemistry 34*, 2832−2843.
40. Miksovska, J., Maroti, P., Tandori, J., Schiffer, M., Hanson, D. K., and Sebban, P. (1996) *Biochemistry 35*, 15411−15417.
41. Maroti, P., Hanson, D. K., Schiffer, M., and Sebban, P. (1995) *Nat. Struct. Biol. 2*, 1057−1059.

42. Nabedryk, E., Brenton, J., Hienderwadel, R., Fogel, C., Mantele, W., Paddock, M. L., and Okamura, M. Y. (1995) *Biochemistry 34*, 14722−14732.
43. Nabedryck, E. (1999) *Biochimic. Biophys. Acta 1411*, 206−213.
44. Sebban, P., Maroti, P., Schiffer, M., and Hanson, D. K. (1995) *Biochemistry 34*, 8390−8397.
45. Hanson, D. K., Tiede, D. M., Nance, S. L., Chang, C., and Schiffer, M. (1993) *Proc. Natl. Acad. Sci. U.S.A. 90*, 8929−8933.
46. Takahashi, E., and Wraight, C. A. (1996) *Proc. Natl. Acad. Sci. USA 93*, 2640−2645.
47. Roussel, A., and Cambillan, C. (1991) *Turbo-Frodo*, Vol. 86, Mountain View, CA.
48. Dunbrack, R. L., and Karplus, M. (1994) *Nat. Struct. Biol. 1*, 334−340.
49. Dunbrack, R. L., and Cohen, F. E. (1997) *Protein Sci. 6*, 1661−1681.
50. Bharadwaj, R., Windemuth, A., Sridharan, S., Honig, B., and Nicholls, A. (1995) *J. Comput. Chem. 16*, 898−913.
51. Nicholls, A., and Honig, B. (1991) *J. Comput. Chem. 12*, 435−445.
52. Sitkoff, D., Sharp, K. A., and Honig, B. (1994) *J. Phys. Chem. 98*, 1978−1988.
53. Parson, W. W., Chu, Z.-T., and Warshel, A. (1990) *Biochim. Biophys. Acta 1017*, 251−272.
54. Wolfenden, R., and Radzicka, A. (1994) *Science 265*, 936−937.
55. Kleinfeld, D., Okamura, M. Y., and Feher, G. (1982) *Biophys. J. 37*, 110a.
56. Hanson, D. K., Baciou, L., Tiede, D. M., Nance, M., Schiffer, M., and Sebban, P. (1992) *Biochim. Biophys. Acta 1102*, 260−265.
57. Wraight, C. A. (1979) *Biochim. Biophys. Acta 548*, 309−327.
58. Kleinfeld, D., Okamura, M. Y., and Feher, G. (1984) *Biochim. Biophys. Acta 766*, 126−140.
59. Labahn, A., Bruce, J. M., Okamura, M. Y., and Feher, G. (1995) *Chem. Phys. 97*, 355−366.
60. Labahn, A., Paddok, M. L., McPherson, P. H., Okamura, M. Y., and Feher, G. (1994) *J. Phys. Chem. 98*, 3417−3423.
61. Paddock, M. L., Axelrod, H. L., Abresch, E. C., Yeh, A. P., Rees, D. C., Feher, D. C., and Okamura, M. Y. (1999) *Biophysical 76*, A141.
62. Abresch, E. C., Paddock, M. L., Stowell, M. H. B., McPhillips, T. M., Axelrod, H. L., Soltis, S. M., Rees, D. C., Okamura, M. Y., and Feher, G. (1998) *Photosynth. Res. 55*, 119−125.
63. Paddock, M. L., Graige, M. S., Feher, G., and Okamura, M. Y. (1999) *Proc. Natl. Acad. Sci. U.S.A. 96*, 6183−6188.
64. Tandori, J., Sebban, P., Michel, H., and Baciou, L. (1999) *Biochemistry 38*, 13179−13187.
65. Paddock, M. L., Feher, G., and Okamura, M. Y. (1995) *Biochemistry 34*, 15742−15750.
66. Warshel, A., and Papazyan, A. (1998) *Current Opinion in Structural Biology 8*, 211−217.
67. Honig, B., and Nicholls, A. (1995) *Science 268*, 1144−1149.
68. Nakamura, H. (1996) *Quart. Rev. Biophys. 29*, 1−90.
69. You, T. J., and Bashford, D. (1995) *Biophys. J. 69*, 1721−1733.
70. Ripoll, D. R., Vorobjev, Y. N., Liwo, A., Vila, J. A., and Scheraga, H. A. (1996) *J. Mol. Biol. 264*, 770−783.
71. Zhou, H., and Vijayakumar, M. (1997) *J. Mol. Biol. 267*, 1002−1011.
72. Beroza, P., and Case, D. (1996) *J. Phys. Chem. 100*, 20156−20163.

BI9929498